Published in final edited form as:
ASAIO J. 2013 ; 59(3): 253–260. doi:10.1097/MAT.0b013e318288a2ab.

Mock Circulatory System of the Fontan Circulation to Study Respiration Effects on Venous Flow Behavior

M. Vukicevic[*], **J.A. Chiulli**[*], **T. Conover**[*], **G. Pennati**[+], **T.Y. Hsia**[#], **R.S. Figliola**[*], and **MOCHA Network**

[*]Department of Mechanical Engineering, Clemson University, Clemson, SC, USA

[+]Laboratory of Biological Structure Mechanics, Politecnico di Milano, Milan, Italy

[#]Great Ormond Street Hospital for Children, NHS Trust, London, UK

Abstract

We describe an *in vitro* model of the Fontan circulation with respiration to study subdiaphragmatic venous flow behavior. The venous and arterial connections of a total cavopulmonary connection (TCPC) test section were coupled with a physical lumped parameter (LP) model of the circulation. Intrathoracic and subdiaphragmatic pressure changes associated with normal breathing were applied. This system was tuned for two patients (5 years, 0.67 m^2; 10 years, 1.2 m^2) to physiological values. System function was verified by comparison to the analytical model on which it was based and by consistency with published clinical measurements. Overall, subdiaphragmatic venous flow was influenced by respiration. Flow within the arteries and veins increased during inspiration but decreased during expiration with retrograde flow in the inferior venous territories. System pressures and flows showed close agreement with the analytical LP model ($p < 0.05$). The ratio of the flow rates occurring during inspiration to expiration were within the clinical range of values reported elsewhere. The approach used to setup and control the model was effective and provided reasonable comparisons with clinical data.

Keywords

respiration; Fontan

INTRODUCTION

We describe an *in vitro* model of the Fontan circulation with respiration so as to study flows in the inferior venous territories. The Fontan circulation refers to a viable pathway in single

Corresponding author: Richard Figliola 247 Fluor Daniel Building Clemson, SC 29634-0921 (864) 656-5635 fgliola@clemson.edu.

MOCHA Investigators:
Andrew Taylor, Alessandro Giardini, Sachin Khambadkone, Silvia Schievano, Marc de Leval, and T.-Y. Hsia (Institute of Cardiovascular Sciences, London, United Kingdom); Edward Bove, and Adam Dorfman, (University of Michigan, Ann Arbor, MI); G. Hamilton Baker and Anthony Hlavacek (Medical University of South Carolina, Charleston, SC); Francesco Migliavacca, Giancarlo Pennati, and Gabriele Dubini (Politecnico di Milano, Milan, Italy); Alison Marsden, (University of California, San Diego, CA); Irene Vignon-Clementel (National Institute of Research in Informatics and Automation, Paris, France); Richard Figliola and John McGregor (Clemson University, Clemson, SC); Jeff Feinstein (Stanford University, Palo Alto, CA).

Disclosures: none

ventricle pathology, where the venous return is surgically routed to the lungs directly without a ventricular pump. Most clinical centers apply the total cavopulmonary connection (TCPC), where the inferior venous return-to-pulmonary artery pathway is streamlined through the atrium or through an extra-cardiac tube.[1] Lacking a ventricular power source, the venous and pulmonary arterial flows become heavily dependent on respiration. Instead of synchronizing with the heart beat, the venous flows are characterized by a phasic pattern,[2-4] where flow is increased during inspiration and decreased in expiration. This pattern is particularly accentuated in the inferior venous return, where the flow can move away from the heart during expiration,[4-7] presumably due to the recoil of the thoracic cage during expiration and the absence of a venous valve.[4] Since many of the late complications of the failing Fontan circulation relate to problems in the liver and gastrointestinal tract, minimizing retrograde flow could improve patient outcomes.[4,6]

This respiration influence has been often reported.[2-9] Figure 1 shows an echocardiogram of hepatic vein flow rate with corresponding respiration volume and ECG, measured on a resting 5.2-year old TCPC patient.[6] The flow rate tracks the low frequency respiration mechanics. During inspiration, indicated by the ascending respiration volume curve, there is a marked increase in hepatic vein flow rate, indicated here by flow tracings below the axis. During expiration, indicated by the descending volume curve, there is a marked decrease in flow rate, including retrograde flow. The ventricular pulse has minimal influence here.

There have been continuing efforts to understand this unique circulation through both numerical and experimental modeling.[10-14] Some findings have led to changes to the operative approach.[12,15,16] Others have demonstrated the effects of geometry on power loss, hepatic vein flow streaming, and pulmonary blood flow distribution.[14-20] Flow studies in steady flow loops describe unsteady, three-dimensional (3D) flow structures.[13,18] Some flow studies have applied a respiration component into the TCPC boundary conditions.[8,26] However, most studies have not included respiration leaving out a major influence on the flow dynamics. Baretta et al.[10,11] described a computational multi-scale model of the complete Fontan circulation with respiration effects, coupling a finite volume model of the TCPC with a lumped parameter network (LP).

The mock circulatory system (MCS) described here is a physical analog of an LP model of the circulation.[11] System function is verified through comparisons of pressure and flow rate measurements to predictions from the analytical model and to comparisons with clinical measurements. Given the heterogeneous nature of the patient population, a realistic model allows predictive studies into patient-specific anomalies and the effects of physiological changes and stresses on the Fontan circulation, such as changes in vascular resistance. By including respiration, a model could provide mechanistic insight into the systems-level pathophysiology of latent Fontan failure, including protein-losing entropathy, liver cirrhosis, and diaphragmatic paralysis.[6] An in vitro model provides a meaningful translation tool to explore new devices[27] and surgical strategies[8] that can potentially improve the performance of the Fontan circulation.

MATERIALS AND METHODS

Mock Circulatory System

The MCS adopts its design from an LP model of the Fontan circulation,[10,11] and includes a 3D TCPC test section. For a practical MCS model, the numbers of individual LP elements describing each branch of circulation were reduced from the host model[11] by applying least-squares impedance matching with Thevenin equivalent circuit analysis. The resulting reduced LP model of Fig. 2 retains the four major branches of circulation: Lower body, Splanchnic, Upper Body (SVC), and Pulmonary. Each branch is described by a single four-

element circuit, including a proximal and a distal resistance, compliance, and inertance element. Baretta et al.[10,11] provide the reference values for the elements, which are scaled by allometric equations to the desired body surface area (BSA). The system was tuned to patient sizes of BSA = 0.67 m^2 (child) and BSA = 1.2 m^2 (adolescent).

Aortic and atrial pressures (P_{ao} and P_{at}) are developed in each of two ways. For direct comparisons to the LP model, constant head tanks are used to supply the mean aortic and mean atrial pressures. For comparisons to clinical measurements, a ventricular assist device (VAD) is used to simulate the single ventricle.

The VAD (Excor®, 80 ml, Berlin, Germany) is supplied fluid from an atrial constant head tank. Pulsatile aortic pressure is developed using a pneumatic pressure switch under computer control. A pulse sequence opens and closes the switch, which supplies the alternating pressures that drive the VAD. Supply pressures are adjusted to control stroke volume while pulse timing controls heart rate and systolic ratio.[28]

Time-dependent respiration pressures associated with normal breathing were applied within thoracic cavity and abdominal elements (P_{th} and P_{ab}). The locations for measurements within the MCS are shown in Fig. 2. A photograph of the physical system is shown in Fig. 3 with components discussed below.

Resistance Elements—Each resistor (R) is realized using either a resistive flow element or an adjustable ball valve. Each flow element consists of a bundle of thin-walled capillary tubes packed within a larger diameter rigid tube to form a honeycomb matrix. Capillary sizes varied from 0.75 to 3 mm diameter (Sutter instruments, Novato, CA) as appropriate.[21] Valves are used upstream of the venous compliances where resistances are relatively large. Resistance values were confirmed by direct measurement *in situ* under steady flow conditions based on $R=\frac{\Delta p}{Q}$, where Δp is the pressure drop across the resistor at flow rate Q. Resistance values are given in Table 1.

Compliance Elements—The upper and lower body compliances are subject primarily to blood pressure variations whereas the pulmonary, splanchnic, and inferior territory compliances are dominated by respiration pressure variations. Accordingly, different designs were used.

The cranial and lower body compliance elements are of the trapped air chamber design.[21] Each consists of an inline closed, rigid cylinder partially filled with air. Compliance is provided by the compressibility of a predetermined volume of trapped air in each 100 mm diameter cylinder. A plumber's test plug (Oatey Corp, Cleveland, OH) traps the air volume, set according to $\forall = CP$. Nominal pressures were 15 mm Hg and variations in pressure (< ±2 mm Hg) were neglected. Compliance in the splanchnic circulation must respond to abdominal (subdiaphragmatic) respiration pressure. To simulate this influence, an elastic, thin-walled latex diaphragm separated the air and liquid phases within an air-chamber element. The air pressure was controlled to reproduce a time-based abdominal respiration pressure. Compliance was set by adjusting the diameter of an orifice restricting the stretching of the diaphragm.

The pulmonary compliance elements consist of two elastic tubes, each tube attached inline to a separate pulmonary artery branch, and both housed within a single sealed air chamber. The inferior vena cava compliance element is similar. Each elastic tube is formed from a pediatric (0.5 L) latex breathing bag. The air pressure in each chamber is controlled to reproduce the sub-atmospheric thoracic cavity respiration pressure. As pressure is varied, the elements stretch expanding with liquid and then relax, simulating respiration. Each

compliance value is set by the length of the bag that is free to stretch. This length is adjusted by placing a stiffer tube around the elastic bag to constrain expansion over a portion of its length. Each element's compliance value was determined by calibration from the slope of $C = f(P, \forall)$. Compliance values used are given in Table 1.

Respiration—Time-varying respiration pressures are developed using programmable proportional pneumatic valves responding to a computer-controlled voltage waveform. Separate valves are used to produce either a vacuum (P_{th}) or compressed (P_{ab}) air pressure waveform (ITV1009, SMC Corp, Noblesville, IN; Tecnobasic, Hoerbinger, GmbH, Altenstadt, Germany).

The respiration waveform applied mimics the rhythm of the clinical waveform of Fig. 1. The respiration activation functions were programmed as

$$P_{th} = \begin{cases} A_{th}\left(\frac{1-\cos\left(2\pi\frac{t}{t_a}\right)}{2}\right) + P_{rest} & t < t_a \\ P_{rest} & t_a \le t < t_R \end{cases} \quad (1)$$

$$P_{th} = \begin{cases} A_{ab}\left(\frac{1-\cos\left(2\pi\frac{t}{t_a}\right)}{2}\right) + P_{rest} & t < t_a \\ P_{rest} & t_a \le t < t_R \end{cases} \quad (2)$$

where A_{th} and A_{ab} are amplitudes of -4 mm Hg and 2 mm Hg for the thoracic and abdominal pressures,[10] respectively. The ratio of the activation function period, t_a, to respiration cycle period, t_R, was 0.375 in all tests. Unless otherwise stated, the respiration rate was 25 bpm (t_R = 2.4 s). P_{rest} was set to atmospheric pressure.

Test Section—The TCPC phantom was based on magnetic resonance (MR) images (BSA = 1.2m^2, male, 10.8 years, 7 years post-LT TCPC) and printed by stereolithography using a transparent rigid resin (Watershed® XC11122; DSM Somos, Elgin, IL).[22] The test section dimensions, as measured 50 mm out from the junction, are: SVC = 13.4 mm, IVC = 24.3 mm, LPA = 11.4 mm, RPA = 11.8 mm.

The LP model assigns a compliance element to the TCPC, whereas the TCPC is rigid in the MCS. We distributed one-half of the TCPC compliance to the proximal IVC and one-quarter to each pulmonary branch. The hepatic vein confluence model was derived from a clinical study.[12] It uses a single 12 mm tube as it enters into the IVC at a 60° angle.

Global Measurements—Instantaneous flow rates are measured using electromagnetic flow probes (P600 probes and Model FM501, Carolina Medical Electronics, King, NC). Flow pressures are measured by wall taps or catheters connected to transducers (DTXplus, BD Medical Systems, Sandy, UT; Model 2120 amplifiers, Micro-measurements Group, Raleigh, NC). Flow and pressure were sampled at 160 Hz/channel (USB 6211 and Labview 8.6; National Instruments, Austin, TX). A saline-glycerin blood analog was used with a density of ρ = 1060 kg/m^3 and kinematic viscosity of 3.3 × 10^{-6} m^2/s.

Uncertainty Estimation—Uncertainties in the pressure and flow rate results are based on instrument error, zero set point error, acquisition error, as well as the statistical standard error from measurement. Zero set-point and instrument errors in the pressure transducers were assumed correlated for pressure differential measurements. Each individual pressure measurement is subject to a ±0.5 mm Hg datum uncertainty. Propagation of uncertainties was done by perturbation and supported by Monte Carlo simulation.[23] Uncertainty in

reported flow rate is about ±0.2% and in differential pressure of ±0.21 mm Hg, each at a 95% level of confidence. The pulmonary, IVC, and splanchnic compliances were set with an uncertainty of ±3.2% (95%), and the other compliance values to within ±1.5% (95%). The uncertainty in each resistance value depended on the measured pressure drop and the flow rate but was under ±5.1% (95%).

RESULTS

Measured pressure and flow values are compared directly to the predictions of the LP model but without ventricular pulsatility so as to verify MCS function.[10,11] Pressure and flow measurements for the case of BSA = 0.67 m^2 are shown in Fig. 4. Signals represent ensemble averages over 25 contiguous cycles. In accordance with Eq. (1) and (2), the applied experimental thoracic respiration pressure decreases with inspiration to P_{th} and increases during expiration to P_{rest} and pauses; the abdominal pressure behaves the opposite. The mean values along with time-based signal variation during respiration, as provided by the standard deviation (SD), are listed in Table 2. The measured and LP model mean TCPC pressures are similar, being within 0.11 mm Hg of each other at 13.22 ± 0.21 mm Hg (95%), indicating that the MCS resistance values were set closely to the intended values. The measured TCPC pressure oscillated more than the model (SD of 0.76 versus 0.55 mm Hg), but otherwise tracked the model behavior closely. The TCPC junction pressure decreased during inspiration and increased during expiration. The pressure in the HV increased then decreased mirroring the abdominal pressure changes. Consequently, the flow rates within the IVC and HV increased with inspiration, then decreased with expiration. The flow rates within the SVC and RPA responded to respiration but with smaller deviations from their mean flows. The IVC and HV flows showed retrograde motion. Measured and predicted mean pressures compare to within ±3% and flow rates to within ±5%; differences between the measured and simulation results are not statistically significant ($p < 0.05$).

Time-dependent measurements for BSA = 1.2 m^2 are given in Fig. 5. Mean values and variations are given in Table 2. The measured TCPC pressure tracked the simulation values closely, decreasing with inspiration and increasing with expiration, and with good agreement in mean value at 14.4 ± 0.21 mm Hg (95%). The pressure in the HV decreased during expiration. Again, the flow rates within the IVC and HV increased with inspiration, then decreased during expiration. The flow rates within the SVC and RPA followed the respiration cycle but the variation was less than in the IVC. The IVC and HV flows both showed retrograde motion, more than for the smaller patient. Measured and predicted mean pressures compare to within ±4% and flow rates to within ±6%, with the largest difference found in the HV. This good agreement using different BSA settings indicates that the MCS will respond in a manner similar to the analytical circulation model.

In Fig. 6, we compare signals measured using respiration only to those using both respiration and ventricular pulsatility (80 bpm, 3.5 Lpm, 40% systolic ratio). Instantaneous signals are shown over one respiration cycle for BSA = 1.2 m^2. The ascending aortic pressure waveform applied and measured is shown (Fig. 6e) while the respiration waveforms (25 bpm) applied remain as presented in Fig. 5. Within the IVC, and hepatic vein, the respiration influence dominates the time-dependent aspects of each flow rate signal, similar to clinical findings.[2-7,9] Ventricular pulsatility is seen as a higher harmonic in IVC and SVC signals. The pressures within the TCPC and liver show the pulsatile signature, but this is much more apparent in the TCPC. The results show the relative importance of including the respiration influence in the study of the subdiaphragmatic regions. The added effect of ventricular pulsatility enriches but does not adversely affect MCS function.

Experimental flow measurements are compared to clinical MR flow measurements for two TCPC patients (1.3 m^2, 10.9 years; 0.66 m^2, 4 years)[8,9]. Experimental respiration rates and VAD cardiac outputs were adjusted to their clinical values (24 and 21 bpm, and 2.81 and 1.92 Lpm, respectively) but other system values retained generic settings (Table 2). The comparisons are shown over one respiration cycle in Fig. 7. For either patient, both the IVC clinical and experimental flows clearly show the respiration influence, including retrograde flow during expiration. Ventricular pulsatility is evident in both signals. For the larger patient, the SVC and RPA flow signals more mildly reflect the respiration waveform with imposed pulsatility. The smaller patient's SVC data shows more pronounced ventricular pulsatility with atrial contraction. This difference is likely due to the patient having a smaller upper body compliance than was modeled. The experimental to clinical mean flows in the IVC compare 1.45 to 1.36, and 1.11 to 1.07 Lpm, for BSA = 1.3 and 0.66 m^2, respectively. In the SVC, the mean flows compare 1.34 to 1.45, and 0.91 to 0.85 Lpm, respectively. Overall, the experimental results track the clinical behaviors reasonably well given the generic settings of the MCS.

DISCUSSION

Hsia et al.[4,6] compared the integrated flow measured during inspiration (Q_{ins}) and during expiration (Q_{exp}) in the subhepatic IVC and HV as a ratio (Q_{ins}/Q_{exp}) in extracardiac TCPC patients (N = 33,10 ± 4 years; N = 28, 7 ± 4 years). Hjordal et al.[5,7] supplemented these measurements using MR velocity mapping (N = 11, 12.4 ± 4.6 years; N = 6, 9.3 ± 2.2 years). We applied methods consistent with either source to achieve a comparable flow ratio. In both MCS models, inspiratory flow is predominant to expiratory flow in the inferior territories, whereas SVC flow shows less respiration dependency. As shown in Table 3, the experimental results are in close agreement with clinical values and fall within their respective standard deviations with only the smaller patient HV flow ratio falling outside this range. There are age and size differences between the patients used in these larger clinical studies and those implied by these limited generic experimental models, but the MCS captures a clinically reasonable response to respiration.

Some additions in the future would supplement the limitations in this model. While generic elemental values were used here, Baretta et al.[10,11] discuss how clinical measurements can be used to adjust the parametric values to be patient-specific. The rigid test section allows for near-term comparisons with computational fluid dynamics simulations but groups are developing physiologically realistic compliant models that include the distributed elastance due to grafts and diseased vessels.[24] Some wave reflections seen clinically are not recreated with rigid test sections.[26] The hepatic vein confluence is extensively variable between patients and we did not study the effects of differing geometries.[12] Respiration has an important influence on the venous flows, but cardiac pulsatility presents a signature in clinical tracings.[25,26] The current system is neither adaptive nor does it incorporate the autoregulatory system inherent to the body. In patients where diaphragmatic function is compromised, the co-relation found between venous flows and respiration would be affected. [6]

CONCLUSION

An experimental model of the Fontan circulation with total cavopulmonary connection and including respiration is described and demonstrated by tuning to two different patient sizes. The approach used proved effective for accurately creating and tuning the resistance, compliance, and respiration elements. The system pressures and flows showed excellent agreement ($p < 0.05$) with the analytical LP model from which it was derived. The pressure and flows showed a direct positive correlation with respiration. The system recapitulated the

existing clinical observation of the respiratory effects of increased antegrade flow with inspiration and decreased flow with expiration, including hepatic venous and IVC flow reversal. The scaled parametric values applied produced flow tracings comparable with published clinical data.

Acknowledgments

Supported by the Leducq Foundation and NIH (grant HL083975).

REFERENCES

1. de Leval MR, Kilner P, Gewillig M, Bull C. Total cavopulmonary connection: a logical alternative to atriopulmonary connection for complex Fontan operations. J Thorac Cardiovasc Surg. 1988; 96:682–695. [PubMed: 3184963]
2. Penny DJ, Redington AN. Doppler echocardiographic evaluation of pulmonary blood flow after the Fontan operation: the role of the lungs. Br Heart J. 1991; 66:372–374. [PubMed: 1747298]
3. Fogel MA, Weinberg PM, Hoydu A, Hubbard A, Rychik J, Jacobs M, Haselgrove J. The nature of flow in the systemic venous pathway in Fontan patients utilizing magnetic resonance blood tagging. J Thorac Cardiovasc Surg. 1997; 114:1032–1041. [PubMed: 9434698]
4. Hsia TY, Khambadkone S, Redington A, Migliavacca F, Deanfield J, deLeval M. Effects of Respiration and Gravity on Infradiaphragmatic Venous Flow in Normal and Fontan Patients. Circulation. 2000; 102:III-148–III-153. [PubMed: 11082378]
5. Hjortdal VE, Emmertsen K, Stenbøg E, Fründ T, Schmidt MR, Kromann O, Sørensen K, Pedersen EM. Effects of Exercise and Respiration on Blood Flow in Total Cavopulmonary Connection. Circulation. 2003; 108:1227–31. [PubMed: 12939218]
6. Hsia TY, Khambadkone S, Bradley S, deLeval M. Subdiaphragmatic venous hemodynamics in patients with biventricular and Fontan circulation after diaphragm placation. J Thorac Cardiovasc Surg. 2007; 134(6):1397–1405. [PubMed: 18023650]
7. Hjortdal V, Christensen T, Larsen S, Emmertsen K, Pedersen E. Caval blood flow during supine exercise in normal and Fontan patients. Ann Thorac Surg. 2008; 85:599–603. [PubMed: 18222273]
8. Yang Y, Feinstein J, Marsden A. Constrained optimization of an idealized Y-shaped baffle. Comp Methods App Mech and Eng. 2010; 199:2135–2149.
9. Sondergaard L, Hoschtitzky A, Hsia T-Y, Deanfield JE, de Leval MR. Respiration synchronized flow quantification in total cavopulmonary connections. Circulation. 2000; 102(18):II–771.
10. Baretta A, Corsini C, Yang W, Vignon-Clementel IE, Marsden AL, Feinstein JA, Hsia TY, Dubini G, Migliavacca F, Pennati G. Virtual surgeries in patients with congenital heart disease: a multiscale modelling test case. Philosophical transactions. Series A. 2011; 369(1954):4316–30.
11. Baretta A, Corsini C, Marsden A, Vignon-Clementel I, Dubini G, Migliavacca F, Pennati G. Respiratory effects in patient-specific CFD models of the Fontan circulation. European J Mech B/ Fluids. 2012; 35:61–69.
12. Hsia TY, Migliavacca F, Pittaccio S, Radaelli A, Dubini G, Pennati G, de Leval M. Computational fluid dynamic study of flow optimization in realistic models of the total cavopulmonary connections. J Surg Res. 2004; 116(2):305–313. [PubMed: 15013370]
13. Pekkan K, de Zelicourt D, Ge L, Sotiropoulos F, Frakes D, Fogel MA, Yoganathan AP. Physics-driven CFD modeling of complex anatomical cardiovascular flows-a TCPC case study. Ann Biomed Eng. 2005; 33(3):284–300. [PubMed: 15868719]
14. Dasi L, Whitehead K, Pekkan K, de Zelicourt D, Sundareswaran K, Kanter K, Yoganathan A. Pulmonary hepatic flow distribution in total cavopulmonary connections: Extracardiac versus intracardiac. J Thorac Cardiovasc Surg. 2011; 141(1):207–214. [PubMed: 20621314]
15. de Leval MR, Dubini G, Migliavacca F, Jalali H, Camporini G, Redington A, Pietrabissa R. Use of computational fluid dynamics in the design of surgical procedures: application to the study of competitive flows in cavo-pulmonary connections. J Thorac Cardiovasc Surg. 1996; 111(3):502–513. [PubMed: 8601964]

16. Ensley AE, Lynch P, Chatzimavroudis GP, Lucas C, Sharma S, Yoganathan AP. Toward designing the optimal total cavopulmonary connection: an in vitro study. Ann Thorac Surg. 1999; 68(4): 1384–1390. [PubMed: 10543511]

17. Pekkan K, Kitajima HD, de Zelicourt D, Forbess JM, Parks WJ, Fogel MA, Sharma S, Kanter KR, Frakes D, Yoganathan AP. Total cavopulmonary connection flow with functional left pulmonary artery stenosis: angioplasty and fenestration in vitro. Circulation. 2005; 112(21):3264–3271. [PubMed: 16286590]

18. de Zélicourt DA, Pekkan K, Wills L, Kanter K, Forbess J, Sharma S, Fogel M, Yoganathan AP. In vitro flow analysis of a patient-specific intraatrial total cavopulmonary connection. Ann Thorac Surg. 2005; 79(6):2094–2102. [PubMed: 15919316]

19. Dasi LP, Krishnankuttyrema R, Kitajima HD, Pekkan K, Sundareswaran KS, Fogel M, Sharma S, Whitehead K, Kanter K, Yoganathan AP. Fontan hemodynamics: importance of pulmonary artery diameter. J Thorac Cardiovasc Surg. 2009; 137(3):560–564. [PubMed: 19258065]

20. Kitajima HD, Sundareswaran KS, Teisseyre TZ, Astary GW, Parks WJ, Skrinjar O, Oshinski JN, Yoganathan AP. Comparison of particle image velocimetry and phase contrast MRI in a patient-specific extracardiac total cavopulmonary connection. J Biomech Eng. 130(4):2008.

21. Kung EO, Taylor CA. Development of a physical windkessel model to recreate in vitro vascular impedance for in vitro experiments. Cardiovascular Engineering and Technology. 2010; 2(1):2–14.

22. Armillotta A, Bonhoeffer P, Dubini G, Ferragina S, Migliavacca F, Sala G, Schievano S. Use of rapid prototyping models in planning of percutaneous pulmonary valved stent implantation. Proc Inst Mech Eng [H]. 2004; 221(4):407–416.

23. Figliola, RS.; Beasley, DE. Theory and Design for Mechanical Measurements. 5th ed.. Wiley; New York: 2005. Chapter 5

24. Biglino G, Verschueren P, Zegels R, Taylor AM, Schievano S. Quantification of TangoPlus FullCure® 930 compliance for printing patient-specific vascular models. ASAIO journal – Abstracts. 2011; 57(2):74.

25. Dur O, Kocyildirium E, Ozlem S, Wearden P, Morell VO, DeGroff C, Pekkan K. Pulsatile venous waveform quality affects the conduit performance in functional and failing Fontan circulations. Cardiology in the Young. 2011; 22(3):251–262. [PubMed: 22008697]

26. Dur O, Keller B, Degroff C, Pekkan K. Optimization of inflow waveform phase-shift for minimized power loss. ASME J Biomech Engr. 2010; 132(2):031012–1.

27. Rodefeld M, Coats B, Fisher T, Giridharan G, Chen J, Brown J, Frankel S. Cavopulmonary assist for the univentricular Fontan circulation: von Kármán viscous impeller pump. J Thorac Cardiovasc Surg. 2010; 14:529–536. [PubMed: 20561640]

28. EXCOR®. Ventricular Assist Device for Pediatric Use. Berlin Heart Inc; The Woodlands, TX: 2011.

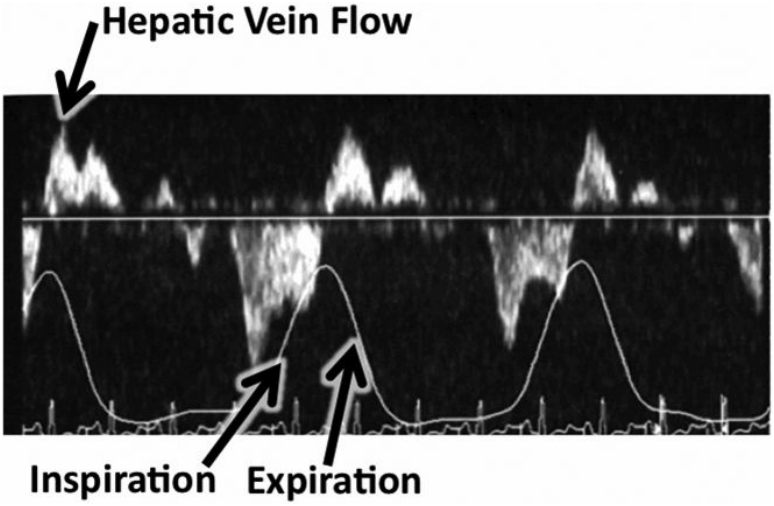

Figure 1.
Echocardiogram tracing (top trace) of hepatic venous flow in a total cavopulmonary connection patient with respiratory volume monitoring (middle trace) and ECG (bottom trace). Forward venous flow is below the x-axis; scales are variable. Ascending respiration trace corresponds to inspiration, while descending curve corresponds to expiration.

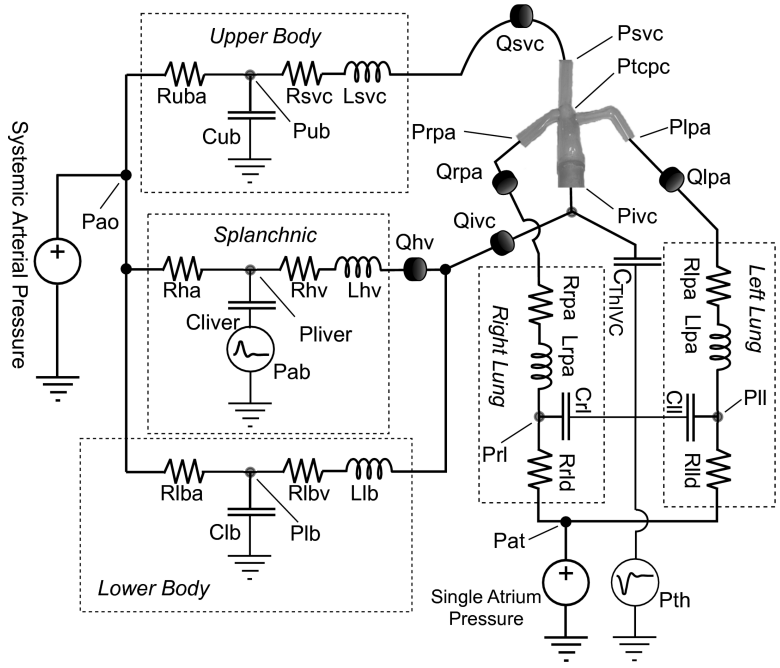

Figure 2.

Reduced lumped parameter network model[10,11] used for the mock circulatory system and measurement points used throughout the system.

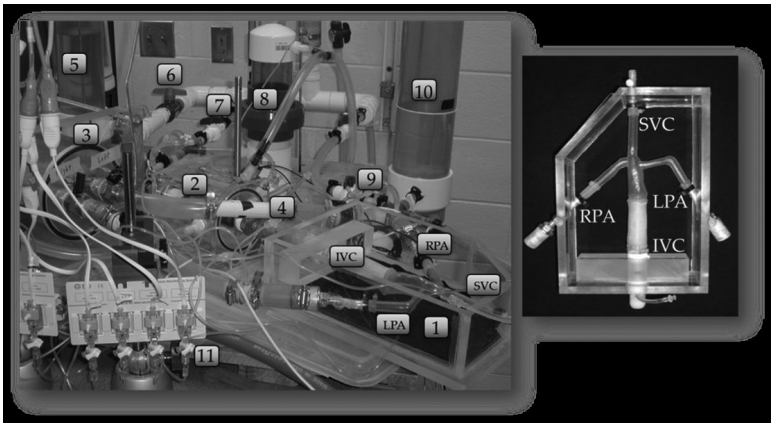

Figure 3.
Photograph of system: 1-TCPC test section (closeup, right), 2 - IVC compliant element, 3 – pulmonary compliance elements, 4 –pulmonary resistance element, 5, 10 – lower and upper body compliance elements, 6, 7, 9 – resistance (valve) elements, 8 – splanchnic compliant element, 11 - pressure transducers.

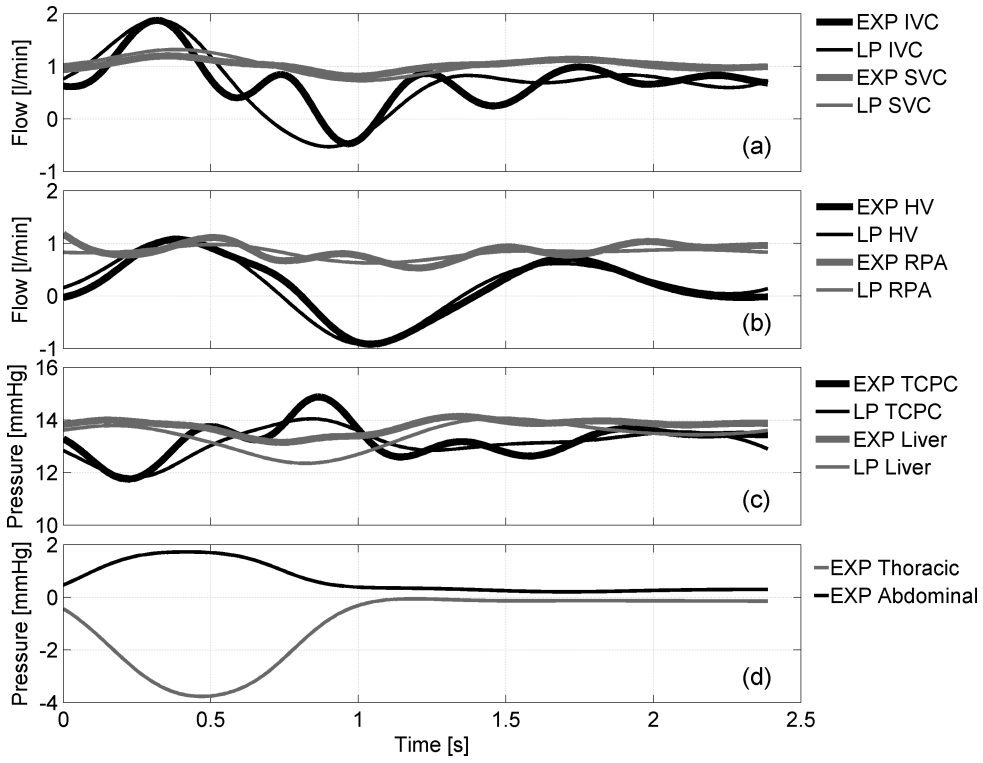

Figure 4.

Comparisons between ensemble averaged experimental (thick lines) and LP model (thin lines) pressure and flow waveforms for the patient with BSA=0.67 m^2.

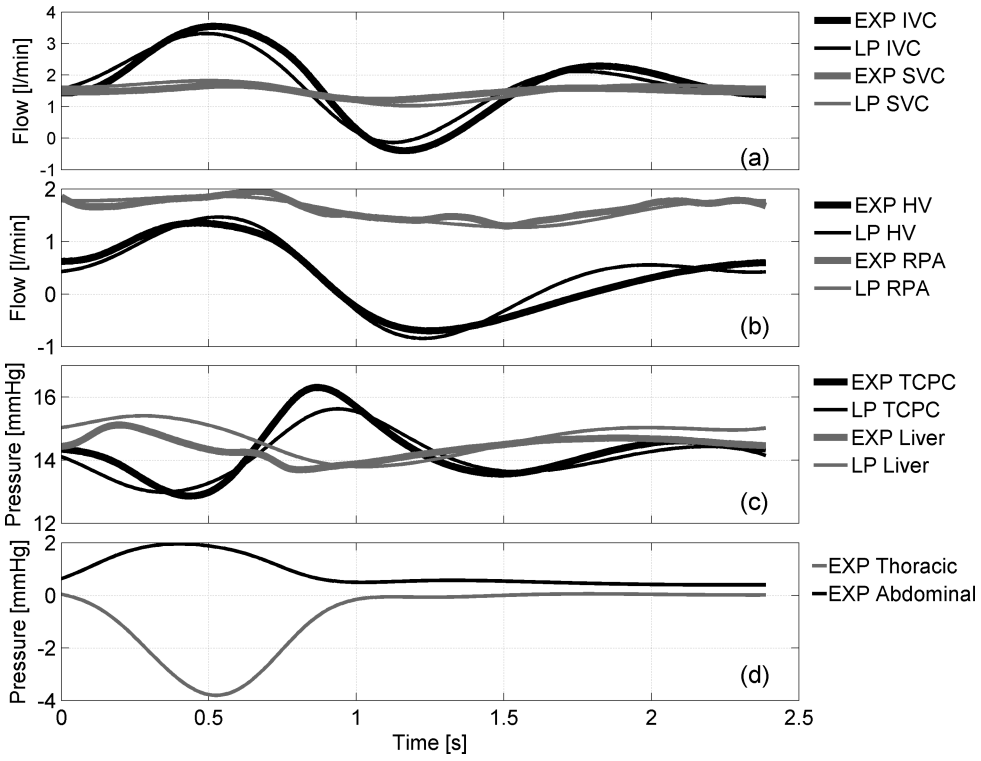

Figure 5.
Comparisons between ensemble averaged experimental (thick lines) and LP model (thin lines) pressure and flow waveforms for the patient with BSA=1.2 m^2.

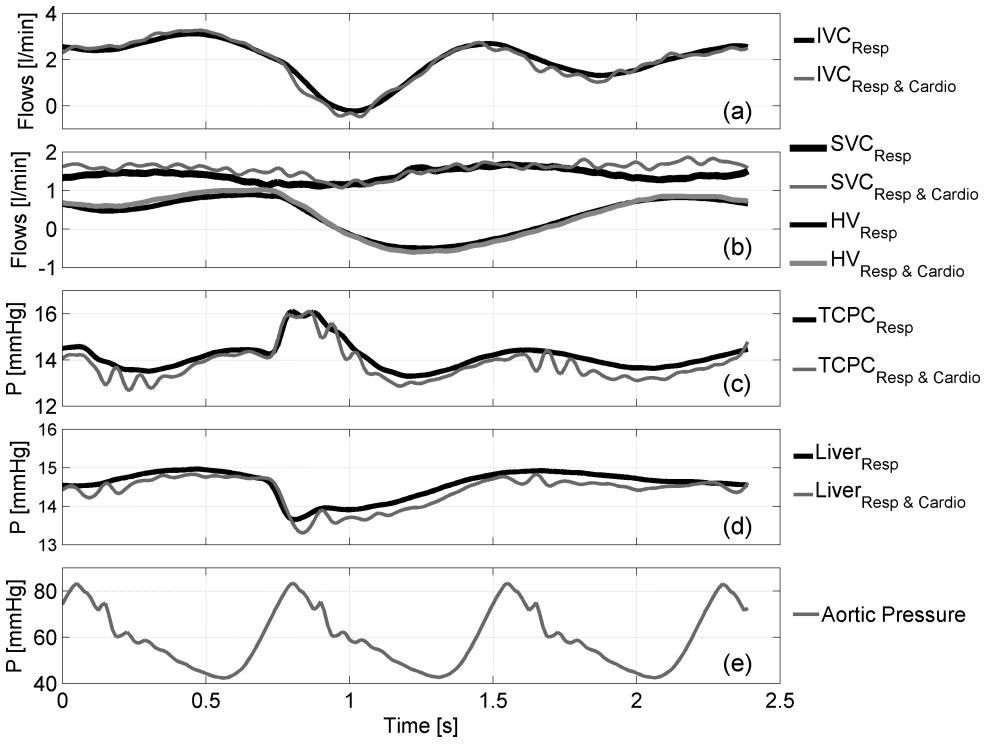

Figure 6.

Instantaneous measured pressure and flow waveforms (BSA= 1.2 m^2) over one respiration cycle: (a) – (d) respiration only applied (black lines), both respiration and ventricular pulsatility applied (gray lines), and (e) the measured ascending aortic pressure associated with ventricular pulsatility.

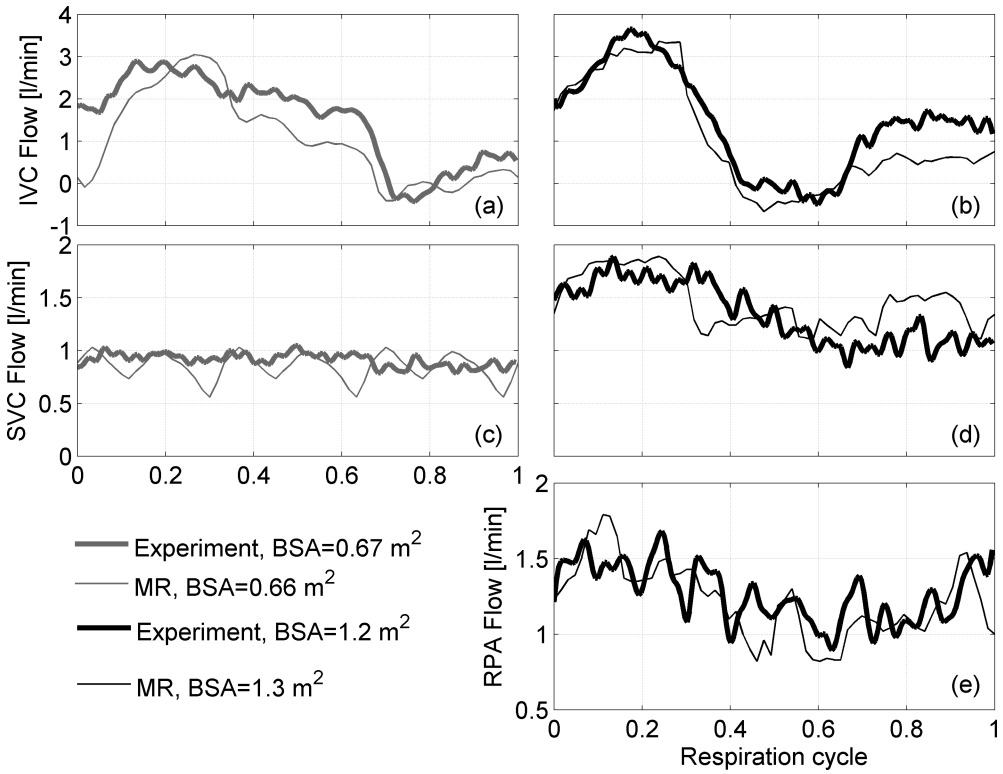

Figure 7.
Clinically measured MR flows[8,9] (BSA = 0.66 m^2 and 1.3 m^2) compared with experimentally measured flows using generic model values (BSA = 0.67 m^2 and 1.2 m^2).

Table 1

LP elemental values achieved in the MCS. Resistance [mmHg * s/ml]; Compliance [ml/mmHg].

	LPN Parameters	Experimental values *
BSA=0.67 m^2	Ruba	1.75 ± 0.08
	Cub	2.15 ± 0.06
	Rsvc	0.11 ± 0.01
	Rha	9.14 ± 0.28
	Cliver	2.17 ± 0.07
	Rhv	0.094 ± 0.005
	Rlba	3.79 ± 0.10
	Clb	1.32 ± 0.013
	Rlbv	0.065 ± 0.003
	Rrpa	0.154 ± 0.008
	Crl	(0.69+0.88/4) ± 0.03
	Rrld	0.326 ± 0.015
	Rlpa	0.154 ± 0.008
	Cll	(0.69+0.88/4) ± 0.03
	Rlld	0.326 ± 0.015
	Ctcpc	0
	Civc	(0.458+0.88/2) ± 0.03
BSA=1.2 m^2	Ruba	1.89 ± 0.09
	Cub	3.12 ± 0.03
	Rsvc	0.08 ± 0.004
	Rha	8.15 ± 0.20
	Cliver	4.41 ± 0.14
	Rhv	0.06 ± 0.003
	Rlba	2.17 ± 0.09
	Clb	3.86 ± 0.06
	Rlbv	0.060 ± 0.003
	Rrpa	0.097 ± 0.005
	Crl	(1.70 +1.76/4) ± 0.066
	Rrld	0.169 ± 0.008
	Rlpa	0.097 ± 0.005
	Cll	(1.70 + 1.76/4) ± 0.066
	Rlld	0.169 ± 0.008
	Ctcpc	0
	Civc	(0.92 + 1.76/2) ± 0.055

* 95% level of confidence

Table 2

Mean flows and pressures along with the variations of the flow about the mean value (calculated as the standard deviation of the signal).

	Mean Flows Q [l/min] Mean Pressures P [mmHg]	BSA=0.67 m^2	BSA=1.2 m^2
Model	Q_{IVC}	0.67±0.60	1.72± 1.11
	Q_{HV}	0.20±0.55	0.34± 0.66
	Q_{SVC}	1.04±0.16	1.47± 0.13
	Q_{RPA}	0.82±0.09	1.63± 0.18
	P_{TCPC}	13.11±0.551	14.28± 0.859
	P_{Liver}	13.40±0.497	14.40± 0.349
	P_{Ao}	53	64
	P_{At}	6.4	7
Experiment	Q_{IVC}	0.70±0.48	1.69± 1.02
	Q_{HV}	0.19±0.55	0.36± 0.70
	Q_{SVC}	1.02±0.10	1.50± 0.26
	Q_{RPA}	0.85±0.16	1.60± 0.18
	P_{TCPC}	13.22±0.759	14.40±0.798
	P_{Liver}	13.80±0.275	15.00± .527
	P_{Ao}	53.0	64.0
	P_{At}	6.4	7.0

Table 3

Inspiratory to expiratory flow ratios as measured in the MCS and compared to available clinical measurements.

		BSA=0.67m^2	BSA=1.2m^2	Clinical data
Flow ratio*	**HV**	1.64[1,2]	1.94[1,2]	3.40 ± 1.53[1]; 3.2 ± 1.3[2]
	SVC	1.07[3]	1.04[3]	1.0 ± 0.23[3]
	IVC	1.80[3]	1.40[3]	1.9 ± 0.5[3]
	Subhepatic IVC	1.17[1,2]	1.00[1,2]	1.32 ± 1.31[1] 1.6 ± 1.7[2]

*MCS values were calculated MCS ratios are stated as an ensemble mean with uncertainty of ± 5% (95%); Clinical values are shown as mean ± SD, as reported in the original articles.

[1]Hsia, 2000

[2]Hsia, 2007

[3]Hjordtal, 2003